Mechanical properties of porous and fully dense low-κ dielectric thin films measured by means of nanoindentation and the plane-strain bulge test technique

Y. Xiang
Division of Engineering and Applied Sciences, Harvard University, Cambridge, Massachusetts 02138

X. Chen
Department of Civil Engineering and Engineering Mechanics, Columbia University, New York, New York 10027

T.Y. Tsui
Texas Instruments Inc., Dallas, Texas 75243

J-I. Jang
Department of Materials Science and Engineering, Hanyang University, Seoul 133-791, South Korea

J.J. Vlassak[a)]
Division of Engineering and Applied Sciences, Harvard University, Cambridge, Massachusetts 02138

(Received 22 July 2005; accepted 1 September 2005)

We report on the results of a comparative study in which the mechanical response of both fully dense and porous low-κ dielectric thin films was evaluated using two different techniques: nanoindentation and the plane-strain bulge test. Stiffness values measured by nanoindentation are systematically higher than those obtained using the bulge test technique. The difference between the measurements is caused by the Si substrate, which adds significantly to the contact stiffness in the indentation measurements. Depending on the properties of the coatings, the effect can be as large as 20%, even if the indentation depth is less than 5% of the film thickness. After correction of the nanoindentation results for the substrate effect using existing models, good agreement is achieved between both techniques. The results further show that densification of porous material under the indenter does not affect stiffness measurements significantly. By contrast, nanoindentation hardness values of porous thin films are affected by both substrate and densification effects. It is possible to eliminate the effect of densification and to extract the yield stress of the film using a model for the indentation of porous materials proposed by the authors. After correcting for substrate and densification effects, the nanoindentation results are in close agreement with the bulge test measurements. The results of this comparative study validate the numerical models proposed by Chen and Vlassak for the substrate effect and by Chen et al. for the densification effect.

I. INTRODUCTION

Over the past several years, a number of materials with low permittivity have been developed to replace SiO_2 as interlayer dielectric in microelectronic devices. The most promising classes of materials are organosilicates and organic polymers. Despite their attractive electrical properties, integrating these newly developed materials has been a slow and difficult process in part because their mechanical properties are inferior compared to SiO_2. They often have an elastic modulus much lower than that of SiO_2. A low modulus reduces the constraint on embedded metal lines and may result in increased susceptibility to electromigration failure. Moreover, the device manufacturing process and normal operation of end-use devices often involve thermal cycles. Polymeric low-κ dielectrics typically have thermal expansion coefficients that are much larger than that of the metal interconnects. This causes large thermal mismatch stresses in both Cu interconnects and dielectrics[1,2] and may result in delamination or even fracture of the dielectric. Organosilicate-based dielectrics frequently have low fracture toughness,

[a)]Address all correspondence to this author.
e-mail: vlassak@esag.deas.harvard.edu
DOI: 10.1557/JMR.2006.0045

making them prone to cracking. The Cu interconnect fabrication process, for instance, involves chemical mechanical planarization (CMP), a process that exposes the dielectric interlayers to a mechanically and chemically rigorous environment.[1–4] If the dielectric lacks sufficient fracture toughness or if it is sensitive to stress-corrosion cracking, failure of the dielectric during this process may be difficult to avoid. These failure mechanisms reduce the yield of the fabrication process as well as the long-term reliability of the end-use devices.[1,2] Thus, measuring the mechanical response of these low-κ materials and understanding their mechanical behavior are critical.

A wide range of techniques is available for the mechanical characterization of thin films.[5,6] These techniques may be divided into two main categories: (i) techniques suitable for testing thin films on substrates and (ii) techniques suitable for measuring freestanding thin films. The first techniques involve minimal sample preparation. Measurements often sample both film and substrate properties, and significant post-processing effort may be needed to extract intrinsic film properties. The second group of techniques requires careful specimen preparation and sample handling but typically yield explicit and accurate film properties.

In the first category, nanoindentation[7,8] is the most widely used and is routinely used within the semiconductor industry to determine stiffness, hardness, and fracture toughness of low-κ dielectric thin films.[3,4,9] Nanoindentation has uncertainties due to well-known experimental limitations that make it difficult to interpret the experimental data accurately. Most notable among these are the effects due to the presence of the substrate already mentioned,[10–12] densification of the film as a result of large hydrostatic stresses,[13,14] issues with tip calibration,[15] surface roughness, and size effects as a result of the inhomogenous strain field.[15] Considerable effort has been devoted to understanding these issues and to relating nanoindentation results to intrinsic material properties. For example, the substrate effect has been studied by Tsui et al.,[16,17] Saha and Nix,[18] Chen and Vlassak,[10] King,[11] Bhattacharya and Nix,[12] and Bolshakov and Pharr.[19] The effect of densification has been discussed by Fleck et al.[14] and Chen et al.[20]

In addition to nanoindentation, a number of dynamic techniques are available for determining the elastic properties of thin films on substrates. These techniques include surface acoustic wave spectroscopy (SAWS)[21] and surface Brillouin scattering (SBS).[22] These techniques typically require knowledge of the density of the film and provide information only on the elastic behavior of the films.

In the second category, the microtensile test[23,24] and the bulge test[25,26] are the most widely used techniques for measuring the mechanical response of thin films. These techniques have been used extensively to study the mechanical behavior of thin metal films. By contrast, there have been relatively few attempts at measuring films with low stiffness, such as low-κ dielectrics, primarily due to difficulties related to fabricating freestanding membranes out of such materials. Martin et al.[27] measured the elastic modulus, the ultimate tensile strength, and the failure strain of an aromatic polymer (SiLK) by uniaxial tensile testing of relatively thick (10 μm) freestanding films. Zheng et al.[28] measured the biaxial moduli of dense and 40%-porosity poly-arylether (PAE) polymeric films by bulge testing of freestanding square membranes. Xiang et al.[13] demonstrated that the stress–strain curve, elastic modulus, residual stress, and ultimate strength of organosilicate glass (OSG) thin films can be measured using the plane-strain bulge test.

In this paper, we extend the work in Ref. 13 and report on a comparative study of the mechanical properties of poly-aromatic and siloxane-based low-κ dielectric thin films measured by means of nanoindentation and the plane-strain bulge test technique. The siloxane-based films are fully dense, but they are much more compliant than the Si substrate; the poly-aromatic films are composed of both dense and porous films. Thus, these materials are ideal for evaluating both substrate and densification effects in nanoindentation. We use the following approach: First nanoindentation is used to evaluate the mechanical response of the coatings as a function of indentation depth and film thickness. This response is compared with the response obtained using the plane-strain bulge test. Substrate and densification effects in nanoindentation are analyzed quantitatively based on numerical models proposed in Refs. 10 and 20. The experimental results obtained using the bulge test and nanoindentation are in good agreement if substrate and densification effects in nanoindentation are properly accounted for.

II. EXPERIMENTAL

A. Materials and sample preparation

In this study, two types of organosilicate glass (OSG) films [denoted as OSG (A) and OSG (B)] and two types of polymeric films (denoted as "dense polymer" and "porous polymer") were prepared. The OSG films were deposited on (100) silicon wafers by means of low-pressure chemical vapor deposition (LPCVD) with octamethylcyclotetrasiloxane (OMCTS) and O_2 as precursors for OSG (A) and tetramethylcyclotetrasiloxane (TMCTS) and O_2 for OSG (B). OSG (A) films had thicknesses ranging from 0.5 to 6.0 μm and OSG (B) films from 0.7 to 3.0 μm. Both fully dense and porous polymer films of 0.85 μm were spin-coated onto (100) silicon wafers with a final cure at 400 °C in N_2 ambient. Nanoindentation specimens were directly cut from the OSG

or polymer-coated substrates; no special sample preparation was required.

To fabricate freestanding membranes for the bulge test, some of the silicon wafers were pre-coated on both sides with 80-nm LPCVD Si_3N_4 prior to deposition of the low-κ dielectric. To protect these films during subsequent processing, the dielectric surface was capped with a plasma-enhanced chemical vapor deposited (PECVD) Si_3N_4 coating, 50 nm thick for OSG (B) films and 30 nm for all other films. Freestanding composite membranes of the LPCVD Si_3N_4/dielectric film/PECVD Si_3N_4 film stack were prepared by opening long rectangular windows in the Si substrate using standard micromachining techniques. A more detailed discussion of the sample preparation process for the bulge test can be found in Ref. 26. Simple polymer membranes were obtained by etching the Si_3N_4 coatings on both sides of the films using reactive ion etching (RIE) with SF_6 as the reactive gas; OSG films were tested in the composite membrane form. In order determine the contribution of the Si_3N_4 bilayers and to extract the OSG properties, freestanding LPCVD Si_3N_4/PECVD Si_3N_4 bilayers of identical thickness were also prepared and tested.

The thickness of the films was measured using an ES-1 Woollam V-VASE32 vertical angle spectroscopic ellipsometer (J.A. Woollam Co., Inc., Lincoln, NE). The results were confirmed using scanning electron microscopy of the film cross sections. The porosity of the porous polymer films was determined to be 0.23 by means of x-ray reflectometry (XRR).

B. Nanoindentation

The nanoindentation samples (OSG and polymer films adherent to Si substrates) were tested using a Nanoindenter XP with a Berkovich indenter tip (MTS System Corporation, Oak Ridge, TN). The Nanoindenter XP was operated in the continuous stiffness measurement[7,8] (CSM) mode by oscillating the load applied to the indenter tip. This mode of operation allows the modulus and hardness to be determined continuously as a function of indentation depth. All indentations were made at a constant nominal strain rate with harmonic oscillation amplitude of 2 nm and a frequency of 45 Hz. The indentation modulus $M = E/(1-\nu^2)$ and hardness H were extracted from the experimental indentation curves using the following equations

$$S = \beta \frac{2}{\sqrt{\pi}} M \sqrt{A} \quad , \tag{1}$$

and

$$H = P/A \quad , \tag{2}$$

after suitable corrections for the finite compliance of the indenter tip and load frame. In these equations, P is the indentation load and A the projected contact area; E and ν are Young's modulus and Poisson's ratio of the material, respectively. The contact stiffness $S = dP/d\delta$ was obtained from the dynamic response of the indenter during the measurement.[8] The projected contact area was calculated from the contact stiffness and applied load as described by Oliver and Pharr;[8] $\beta \approx 1.034$ is a correction factor for the Berkovich indenter.[11]

C. Plane-strain bulge test

Figure 1 presents a schematic illustration of the plane-strain bulge test technique. In this technique, a freestanding film of interest is deformed in plane strain by applying a uniform pressure to one side of a rectangular membrane made out of the thin-film material. If the aspect ratio of the membrane exceeds four,[25,26] the strain imposed in the longitudinal direction of the membrane [axis 2 in Fig. 1(b)] is nearly zero, and the membrane is in a state of plane strain. Loading is essentially quasistatic with a nominally constant strain rate on the order of 10^{-6} s^{-1}. The applied pressure p and the corresponding membrane deflection h are measured and converted into the stress–strain curve of the film using the following analytical formulae[25,26]

$$\sigma = \frac{p(a^2 + h^2)}{2ht} \quad , \tag{3}$$

and

$$\epsilon = \epsilon_0 + \frac{a^2 + h^2}{2ah} \arcsin\left(\frac{2ah}{a^2 + h^2}\right) - 1 \quad , \tag{4}$$

where t is the film thickness, $2a$ the membrane width, and ϵ_0 the residual strain in the film.

Three types of samples [freestanding polymer films, composite membranes with OSG (A) or (B), and LPCVD Si_3N_4/PECVD Si_3N_4 bilayers] were tested in a bulge test

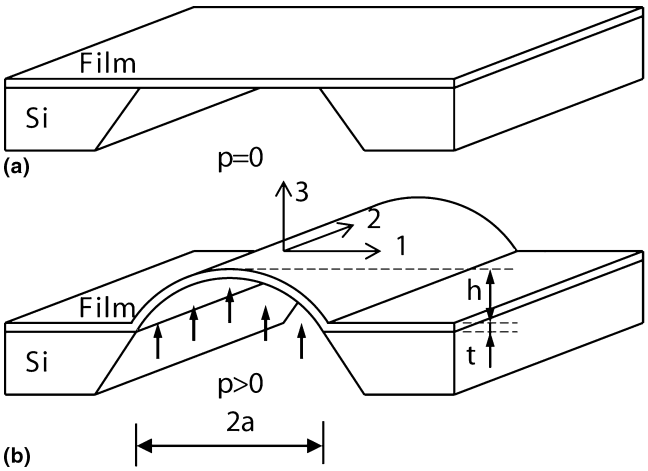

FIG. 1. Perspective views of a bulge test sample (a) before and (b) after a uniform pressure is applied.

apparatus with a pressure resolution of 0.1 kPa and a deflection resolution of 0.3 μm. A detailed description of the experimental system can be found in Ref. 26. For the freestanding polymer films, the pressure–deflection curves can be directly converted into stress–strain curves using Eqs. (3) and (4). For the Si_3N_4/OSG/Si_3N_4 composite films, the elastic contribution of the Si_3N_4 layers needs to be subtracted first. This was done according to the procedure described in Ref. 29: First, the mechanical response of the Si_3N_4 bilayer membranes was measured. The pressure–deflection curves of these bilayer membranes were then subtracted from those of the composite films, and the resulting curves were converted into stress–strain curves for the OSG using Eqs. (3) and (4). The residual stress, elastic modulus, and ultimate strength of the dielectric films can be readily determined from the respective stress–strain curves.

III. RESULTS AND DISCUSSIONS

A. Nanoindentation results

The indentation modulus and hardness obtained from the nanoindentation experiments are presented as a function of normalized indentation depth δ/t for the OSG films in Fig. 2. It is evident from Fig. 2(a) that the indentation modulus of all OSG coatings decreases with decreasing indentation depth. This trend is caused by the presence of the Si substrate, which is much stiffer than the OSG films and which contributes significantly to the indentation contact stiffness if the indentation depth is a large fraction of the film thickness. It is generally assumed that substrate effects become insignificant when the indentation depth is less than 10% of the film thickness.[30] The results in Fig. 2(a), however, show that the experimental values of the indentation moduli continue to decrease, albeit more slowly, at these shallow depths. The intrinsic indentation modulus may then be estimated from the asymptotic value at low penetration depths (see Table I). This observation is confirmed by the fact that the intrinsic indentation moduli do not vary significantly with film thickness. The hardness data in Fig. 2(b) follow the same trend as the indentation moduli, even though the substrate effect is not quite as large.

Figures 3(a)–3(c) illustrate the mechanical response of the polymer coatings in the nanoindentation experiments. Typical load–displacement curves for porous and fully dense films are shown in Fig. 3(a). The trends of indentation modulus [Fig. 3(b)] and hardness [Fig. 3(c)], with indentation depth are similar to those observed for the OSG coatings. This is not surprising given the large difference in properties between substrate and coatings. The figures also give a good indication of the effect of the porosity on the behavior of the films. Introduction of 23% porosity in the polymer films reduces both the indentation modulus and the hardness of the coating by approximately 30%. The experimental values (Table II) are lower than expected based on a simple rule of mixtures. It should be noted, however, that the large hydrostatic pressure associated with indentation may cause

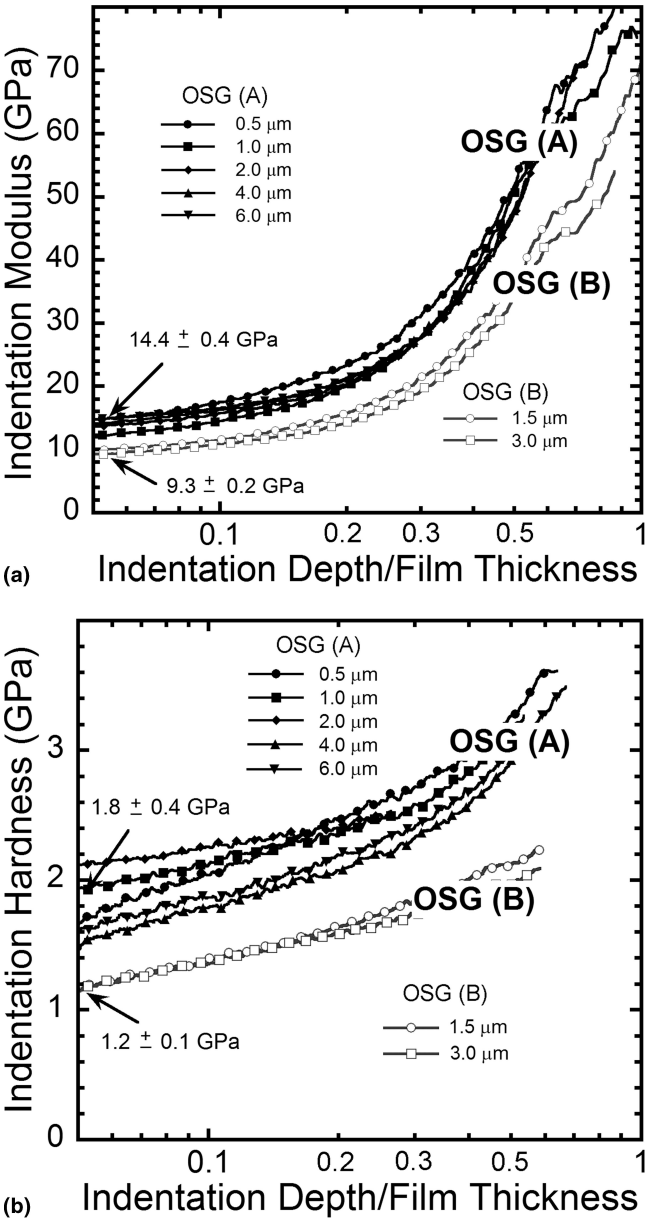

FIG. 2. (a) Indentation modulus and (b) hardness as a function of the normalized indentation depth for OSG (A) and OSG (B) films with a range of thicknesses.

TABLE I. Summary of the experimental results for the OSG films.

	Plane-strain modulus (GPa)		
		Nanoindentation	
Film type	Bulge test	Measured	Corrected[a]
OSG (A)	12.7 ± 0.5	14.4 ± 0.4	13.0 ± 0.4
OSG (B)	8.4 ± 0.5	9.4 ± 0.4	8.4 ± 0.4

[a]Results corrected for the presence of the substrate.

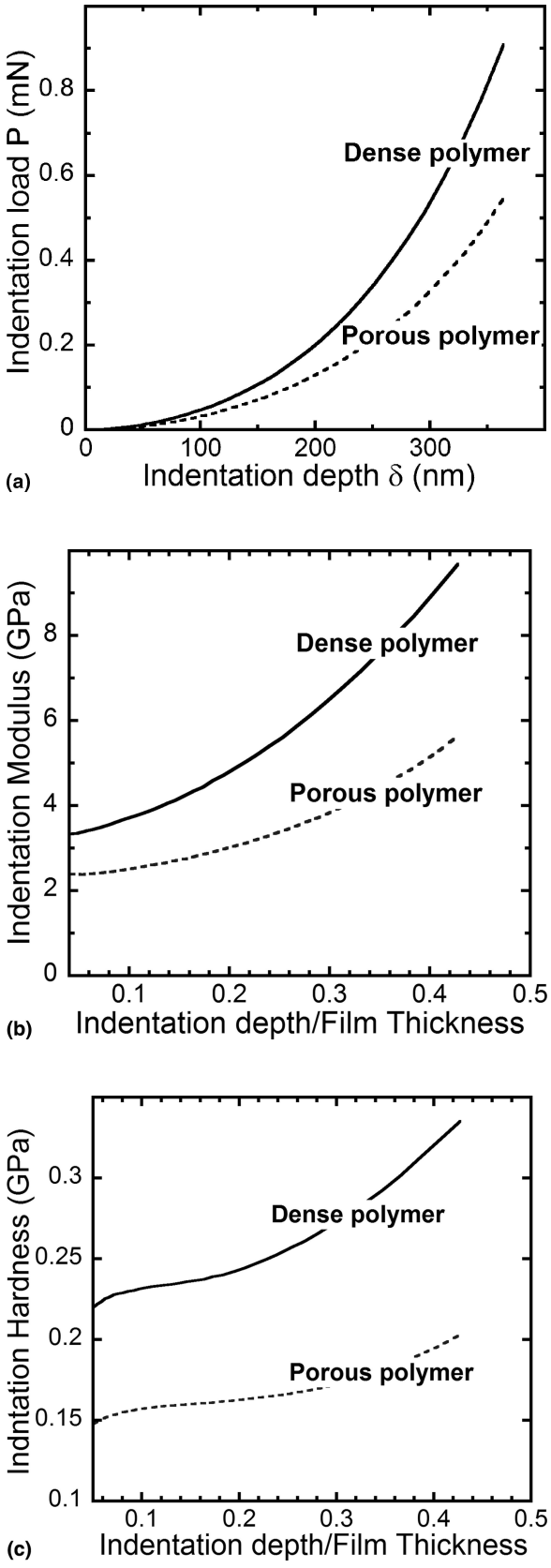

FIG. 3. Comparison of (a) the load–displacement curve, as well as (b) the indentation modulus and (c) hardness as a function of normalized indentation depth for fully dense and porous polymer thin films.

some pores to collapse creating a region of reduced porosity underneath the indenter tip. This densification could lead to an overestimation of the indentation modulus and hardness of the coatings; i.e., the indentation measurements should in effect be regarded as upper bounds to the actual values. The issue of densification will be further explored Sec. III. C.

B. Plane-strain bulge test results

Figures 4(a) and 5(a) show the mechanical response of the OSG composite membranes for various values of OSG thickness, along with the deflection curves for the Si_3N_4 bilayers. The corresponding stress–strain curves are presented in Figs. 4(b) and 5(b). The OSG coatings deform linearly elastically over the entire range of strains in the experiments and eventually rupture at strains as large as 1%. The slopes of the stress–strain curves are the plane-strain moduli of the coatings, $M = E/(1 - \nu^2)$ (see Table I); the experimental values of the plane-strain moduli for both types of OSG are plotted in Fig. 6 along with the indentation moduli.

Figure 7(a) presents typical pressure-deflection curves for the 0.85 μm dense and porous polymer films; the corresponding plane–strain stress–strain curves are shown in Fig. 7(b). The stress–strain curve of the dense polymer is highly nonlinear; the unloading cycle shows significant hysteresis, although it is difficult to ascertain how much of the hysteresis is due to plastic or anelastic deformation. The plane–strain moduli of the coatings are determined from linear fits to the initial sections of the stress-strain curve and are listed in Table II along with the nanoindentation results.

The hardness of an ideally plastic material is directly related to its yield stress through an appropriate proportionality constant. To compare the hardness of a work-hardening solid with its flow stress, one needs to define the flow stress at an appropriate representative strain that depends on the shape of the indenter.[31] For Berkovich indenters, this representative strain is approximately 7%. Since the polymer coatings rupture at smaller strains, the rupture stress is used as the representative flow stress instead. The corresponding values are listed in Table I. They should be regarded as lower bounds to the actual values, which should be quite close for at least the fully dense polymer. The relationship between hardness and yield stress will be investigated in more detail in the next section.

C. Comparison and discussion

For isotropic materials, the indentation modulus M is equal to the plane-strain modulus, $E/(1 - \nu^2)$, of the material and is therefore directly comparable with the stiffness value obtained in the plane-strain bulge test. Figure 6 compares the indentation moduli of both types

TABLE II. Summary of the experimental results for the polymer films.

	Plane-strain modulus (GPa)			Strength (MPa)		
		Nanoindentation		Bulge test	Nanoindentation	
Film type	Bulge test	Measured	Corrected[a]	σ_y[b]	Hardness[c]	σ_y
Fully dense	2.7 ± 0.1	3.4 ± 0.2	2.7 ± 0.2	93 ± 4	231 ± 5	115 ± 3
23% porosity	2.0 ± 0.1	2.4 ± 0.3	1.9 ± 0.3	>55 ± 3	158 ± 5	86 ± 3

[a]Results corrected for the presence of the substrate.
[b]Rupture stress in the bulge test.
[c]Hardness values are taken at an indentation depth of 10% of the film thickness.

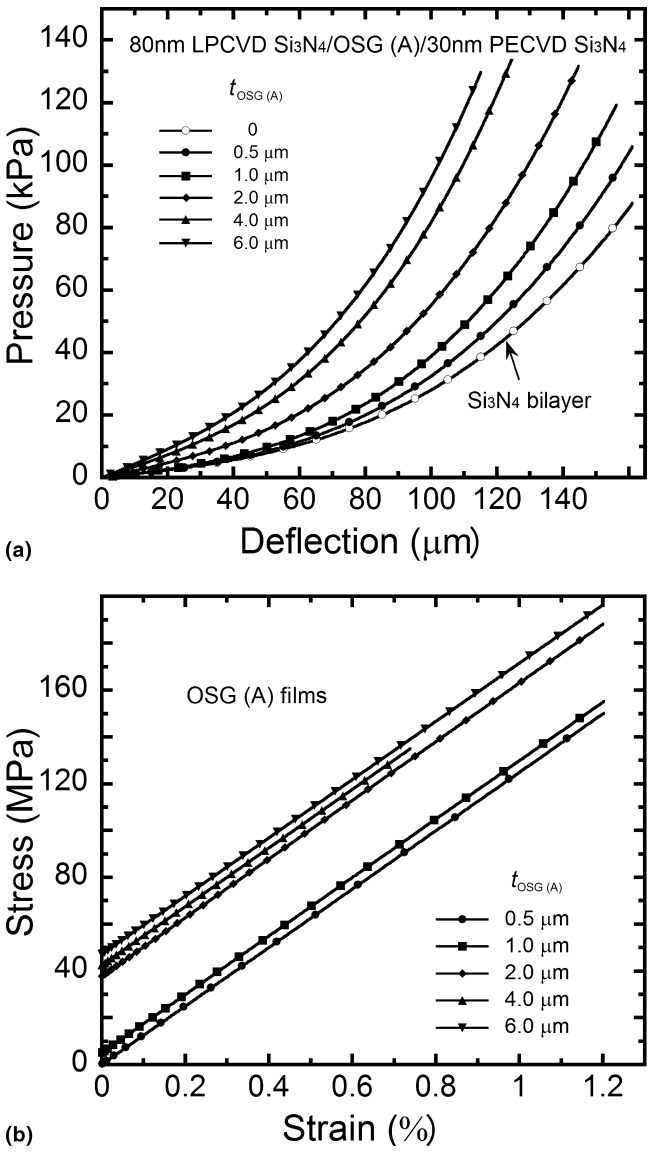

FIG. 4. Bulge test results for OSG (A) films of 0.5–6.0 μm: (a) the pressure-deflection curves of the freestanding composite membranes [80 nm LPCVD Si_3N_4/OSG (A)/30 nm PECVD Si_3N_4] and the Si_3N_4 bilayers [80 nm LPCVD Si_3N_4/30 nm PECVD Si_3N_4]; (b) the stress–strain curves of the OSG (A) films. The stress–strain curves are offset as a result of differences in the residual stress in the membranes.

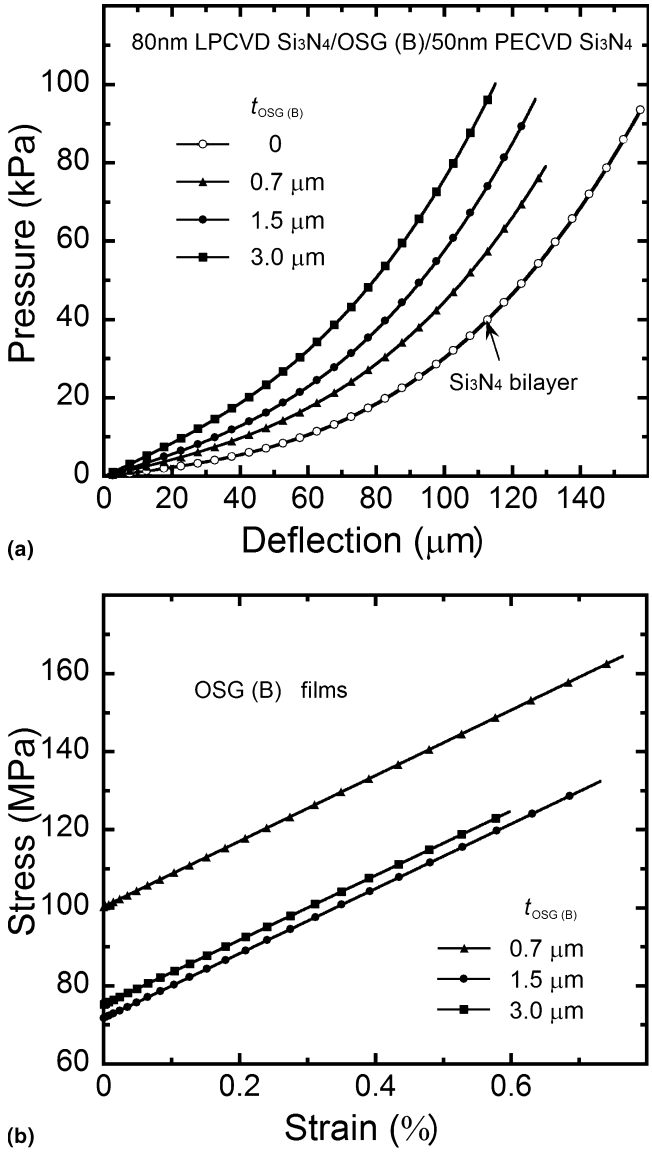

FIG. 5. Bulge test results for OSG (B) films of 0.7–3.0 μm: (a) the pressure-deflection curves of the freestanding composite membranes [80 nm LPCVD Si_3N_4/OSG (B)/50 nm PECVD Si_3N_4] and the Si_3N_4 bilayers [80 nm LPCVD Si_3N_4/50 nm PECVD Si_3N_4]; (b) the stress–strain curves of the OSG (B) films. The stress–strain curves are offset as a result of differences in the residual stress in the membranes.

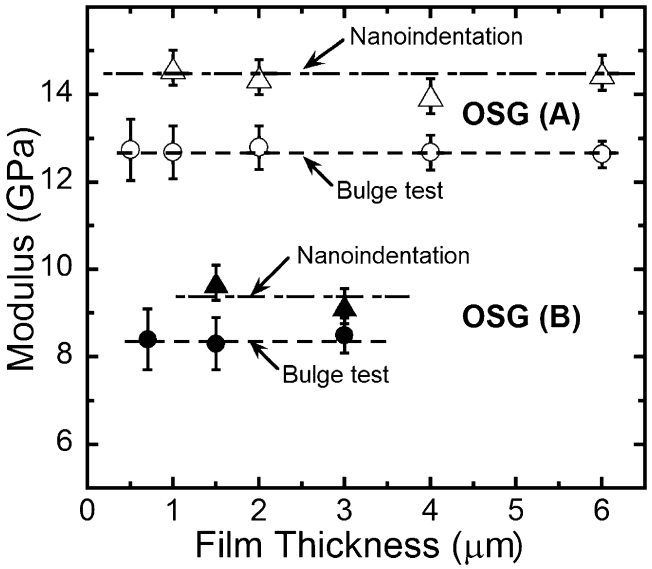

FIG. 6. Comparison of the plane-strain moduli of the OSG (A) and OSG (B) films measured using nanoindentation and bulge testing.

of OSG with the plane-strain moduli obtained using the bulge test. For both techniques, the stiffness values are independent of film thickness. The nanoindentation results are approximately 12% larger than the bulge test results. This difference is due to the substrate effect, which is not negligible even at small indentation depths.[10] Using a stiffness correction map (Fig. 10 in Ref. 10) and an indentation depth of 5% of the film thickness, the substrate effect is calculated to increase the experimental indentation moduli by 10%, in good agreement with the experimental results (Table I). It should further be noted that OSG (A) is significantly stiffer than OSG (B), even though the precursor used for the former contains more methyl groups. The stiffness of OSG coatings is often correlated with the presence of methyl groups in the siloxane network, with more methyl groups leading to a more compliant material.[32] Clearly a detailed analysis of the structure of the OSG coatings is required to understand the difference in stiffness.

Table II compares the stiffness of dense and porous polymer films obtained by the bulge test and nanoindentation. The moduli measured using nanoindentation are higher than the values obtained from the bulge test for both polymers. The difference can again be attributed to the presence of the substrate in the nanoindentation measurements. Using the stiffness correction maps in Ref. 10, the effect of the substrate on the experimental indentation moduli is calculated to be approximately 20%, in good agreement with the measurements (see Table II). Moreover, the results confirm an observation by Chen et al.,[20] who used a finite element model to demonstrate that densification has no significant effect on the measurement of the indentation modulus.

As mentioned in the previous section, the hardness of

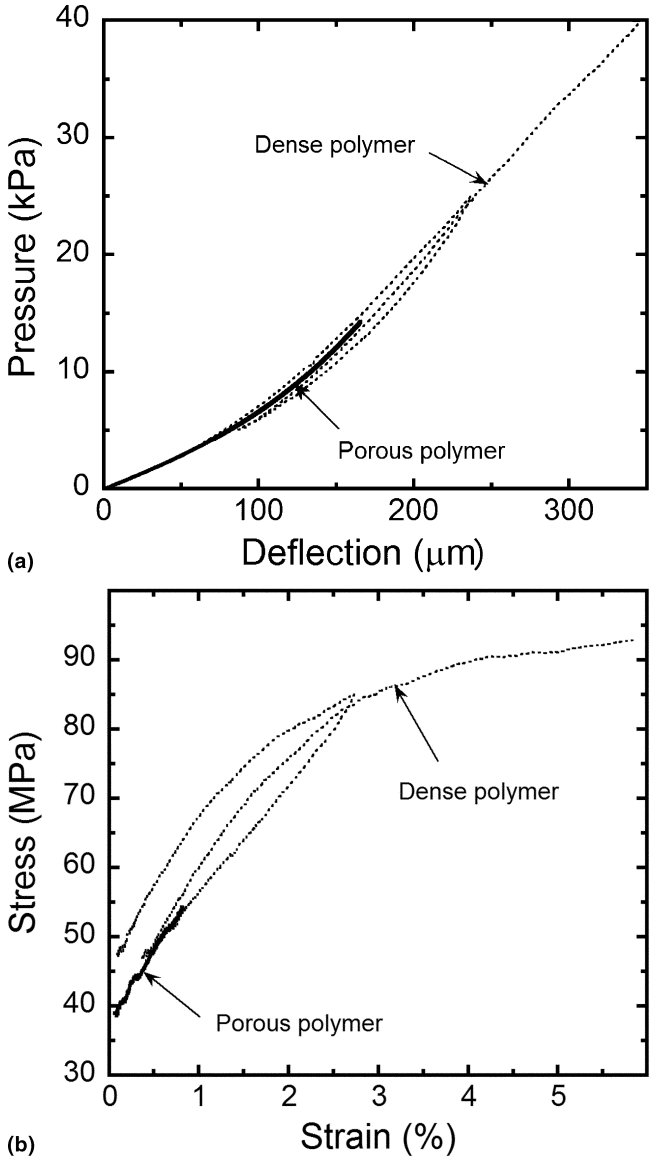

FIG. 7. Bulge test results for freestanding dense and porous polymer films of 0.85 μm: (a) pressure-deflection curves and (b) stress–strain curves.

an ideally plastic material is related to its yield stress σ_y through a proportionality factor

$$H = c_b \sigma_y \quad . \tag{5}$$

Here the proportionality factor c_b depends on material properties and indenter shape: c_b increases with $\bar{E}\tan\alpha/\sigma_y$ and approaches a constant value (≈ 3) when $\bar{E}\tan\alpha/\sigma_y > 30$, where α is the angle of the indenter.[10,33] If the material work hardens, the flow stress at a representative strain should be used instead.[31]

For porous thin films, the hardness as determined from Eq. (2) is depth-dependent because of the substrate effect. Moreover, the high hydrostatic stress underneath the indenter causes the material underneath the indenter to

densify as a result of pore collapse. Equation (5) is based on traditional plasticity in which the density of a material is not changed by plastic flow. This assumption is clearly not valid for porous materials. It is possible, however, to relate experimental hardness values to intrinsic material properties of the film using the procedure described in detail in the companion paper.[20] First, a correction is made for the effect of the substrate using the hardness maps in Ref. 10. This procedure eliminates the effect of the substrate on the experimental data and yields the hardness value for a bulk sample made of the same porous material as the film.

Next, the properties of an equivalent fully dense material are determined using a conversion factor derived from the Gurson model for the plastic deformation of porous media[20]

$$c^{\mathrm{P}} = H_{\mathrm{b}}^{\mathrm{P}}/\sigma_{\mathrm{y}}^{\mathrm{D}} \quad , \tag{6}$$

where $\sigma_{\mathrm{y}}^{\mathrm{D}}$ is the intrinsic yield stress of the fully dense material. This conversion factor depends on the degree of porosity and on the material properties; its numerical values are given in Ref. 20. Figure 8(a) shows the conversion factor as a function of $E^{\mathrm{P}}/\sigma_{\mathrm{y}}^{\mathrm{D}}$ and porosity f. The physical meaning of the equivalent fully dense material is that it represents the material in the ligaments of the porous material. For a material that does not show any size effects or for length scales where size effects are not important, one would expect the equivalent fully dense material to have the same properties as the bulk material without porosity. The yield stress of the porous material can then be estimated from the yield stress of the equivalent fully dense material using the Gurson model. Figure 8(b) shows the yield stress of the porous material as a function of pore volume fraction. It should be noted that in this analysis the interaction between densification, and the presence of a substrate has been ignored. This interaction arises when the substrate alters the level of hydrostatic stress under the indenter and will be investigated in detail in the near future.

We now apply this analysis to the hardness results obtained for the polymeric films. For the fully dense polymer films, the conversion coefficient is found to be approximately 2.0, while for films with a porosity of 23%, it is 1.4. Thus the hardness of the fully dense film corresponds to a yield stress of 115 MPa for the dense polymer, while the hardness of the porous film leads to a value of 113 MPa. The agreement between both measurements is quite remarkable. Moreover, the nanoindentation measurements are also close to the yield stress of 93 MPa obtained for the fully dense polymer using the bulge test technique. These results suggest that the presence of pores does not change the yield stress of the matrix in the porous films; i.e., there is no size effect in the matrix material. It is further possible to determine the yield stress of the porous polymer from these results and the conversion chart in Fig. 8(b). The yield stress of a polymer film with 23% porosity is found to be approximately 86 MPa. The porous membrane ruptured in the bulge test at a stress of 55 MPa before extensive plastic deformation could take place, providing a lower bound for the yield stress of the porous polymer. The agreement between the experimental results obtained using the nanoindentation and the bulge test techniques seems to validate the analysis of nanoindentation results for porous materials proposed by Chen et al.[20]

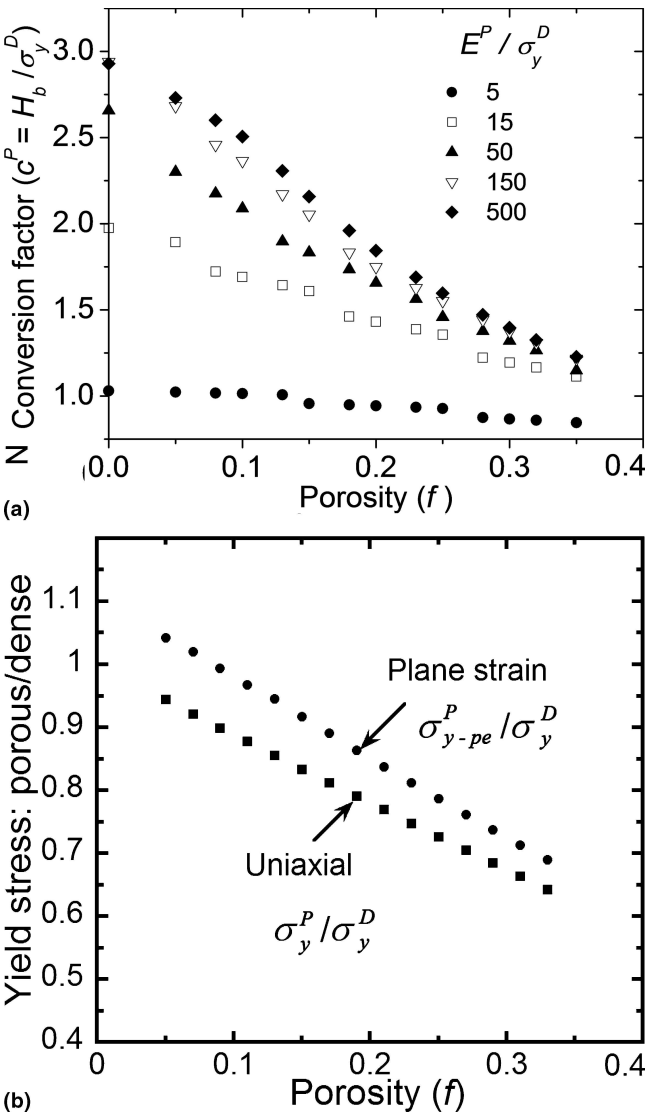

FIG. 8. Correction of densification effects in nanoindentation on porous materials[20]: (a) conversion factor c^{P} as a function of the stiffness to yield stress ratio and porosity and (b) yield stress map obtained using Gurson's model.

IV. CONCLUSIONS

The mechanical response of a number of fully dense and porous low-κ dielectric thin films with thicknesses

ranging from half a micron to several microns have been measured by means of nanoindentation and the plane-strain bulge test. The stiffness measurements by nanoindentation are systematically higher than those obtained using the bulge test technique as a result of the presence of the stiff Si substrate. After correction of the nanoindentation results for the substrate effect using existing models, good agreement is achieved between both techniques. Densification of the material under the indenter does not affect the stiffness measurement significantly for porous films. By contrast, the hardness values of porous thin films obtained using nanoindentation are affected by both substrate and densification effects. Using conversion factors based on the Gurson model and a simple yield stress map, it is possible to extract the yield stress of the fully dense and porous films from the nanoindentation measurements. The results from this analysis are very close to independent measurements obtained using the bulge test technique. The good agreement between the bulge test and nanoindentation measurements after substrate and densification effects have been properly taken into account validates the numerical models for the substrate effect proposed by Chen and Vlassak[10] and for the densification effect by Chen et al.[20]

ACKNOWLEDGMENTS

This work was supported primarily by the Materials Research Science and Engineering Center of the National Science Foundation under NSF Award No. DMR-0213805 and by the Semiconductor Research Corporation (Task ID 1292.010). X.C. acknowledges support from NSF Award No. CMS-04077432. The authors would like to thank George Pharr for use of the nanoindenter.

REFERENCES

1. M. Morgen, E.T. Ryan, J.H. Zhao, C. Hu, T.H. Cho, and P.S. Ho: Low-dielectric constant materials for ULSI interconnects. *Annu. Rev. Mater. Sci.* **30,** 645 (2000).
2. K. Maex, M.R. Baklanov, D. Shamiryan, F. Iacopi, S.H. Brongersma, and Z.S. Yanovitskaya: Low-dielectric constant materials for microelectronics. *J. Appl. Phys.* **93,** 8793 (2003).
3. A.A. Volinsky, J.B. Vella, and W.W. Gerberich: Fracture toughness, adhesion and mechanical properties of low-K dielectric thin films measured by nanoindentation. *Thin Solid Films* **429,** 201 (2003).
4. J.B. Vella, I.S. Adhihetty, K. Junker, and A.A. Volinsky: Mechanical properties and fracture toughness of organo-silicate glass (OSG) low-k dielectric thin films for microelectronic applications. *Int. J. Fract.* **119,** 487 (2003).
5. W.D. Nix: Mechanical properties of thin films. *Metall. Trans. A* **20,** 2217 (1989).
6. R.P. Vinci and J.J. Vlassak: Mechanical behavior of thin films. *Annu. Rev. Mater. Sci.* **26,** 431 (1996).
7. W.C. Oliver and G.M. Pharr: Measurement of hardness and elastic modulus by instrumented indentation: Advances in understanding and refinements to methodology. *J. Mater. Res.* **19,** 3 (2004).
8. W.C. Oliver and G.M. Pharr: An improved technique for determining hardness and elastic-modulus using load and displacement sensing indentation experiments. *J. Mater. Res.* **7,** 1564 (1992).
9. J. Malzbender, J.M.J. den Toonder, A.R. Balkenende, and G. de With: Measuring mechanical properties of coatings: A methodology applied to nano-particle-filled sol-gel coatings on glass. *Mater. Sci. Eng. R—Rep.* **36,** 47 (2002).
10. X. Chen and J.J. Vlassak: Numerical study on the measurement of thin film mechanical properties by means of nanoindentation. *J. Mater. Res.* **16,** 2974 (2001).
11. R.B. King: Elastic analysis of some punch problems for a layered medium. *Int. J. Solids Struct.* **23,** 1657 (1987).
12. A.K. Bhattacharya and W.D. Nix: Analysis of elastic and plastic-deformation associated with indentation testing of thin-films on substrates. *Int. J. Solids Struct.* **24,** 1287 (1988).
13. Y. Xiang, T.Y. Tsui, J.J. Vlassak, and A.J. McKerrow: Measuring the elastic modulus and ultimate strength of low-κ dielectric materials by means of the bulge test, in *Proc. IEEE Int. Interconnect Tech. Conf.*, edited by IEEE (IEEE, Piscataway, NJ, 2004), p. 133.
14. N.A. Fleck, H. Otoyo, and A. Needleman: Indentation on porous solids. *Int. J. Solids Struct.* **29,** 1613 (1992).
15. K.W. McElhaney, J.J. Vlassak, and W.D. Nix: Determination of indenter tip geometry and indentation contact area for depth-sensing indentation experiments. *J. Mater. Res.* **13,** 1300 (1998).
16. T.Y. Tsui, J.J. Vlassak, and W.D. Nix: Indentation plastic displacement field: Part I. The case of soft films on hard substrates. *J. Mater. Res.* **14,** 2196 (1999).
17. T.Y. Tsui, J.J. Vlassak, and W.D. Nix: Indentation plastic displacement field: Part II. The case of hard films on soft substrates. *J. Mater. Res.* **14,** 2204 (1999).
18. R. Saha and W.D. Nix: Effects of the substrate on the determination of thin film mechanical properties by nanoindentation. *Acta Mater.* **50,** 23 (2002).
19. A. Bolshakov and G.M. Pharr: Influences of pileup on the measurement of mechanical properties by load and depth-sensing indentation techniques. *J. Mater. Res.* **13,** 1049 (1998).
20. X. Chen, Y. Xiang, and J.J. Vlassak: A novel technique of measuring the mechanical properties of porous materials by nanoindentation: With application to low-k dielectric thin films. *J. Mater. Res.* (submitted) (2006).
21. G.W. Farnell and E.L. Adler: *Physical Acoustics* (Academic Press, New York and London, 1972).
22. G. Carlotti, L. Doucet, and M. Dupeux: Comparative study of the elastic properties of silicate glass films grown by plasma enhanced chemical vapor. *J. Vac. Sci. Technol. B* **14,** 3460 (1996).
23. H.B. Huang and F. Spaepen: Tensile testing of free-standing Cu, Ag and Al thin films and Ag/Cu multilayers. *Acta Mater.* **48,** 3261 (2000).
24. D.T. Read and J.W. Dally: A new method for measuring the strength and ductility of thin-films. *J. Mater. Res.* **8,** 1542 (1993).
25. J.J. Vlassak and W.D. Nix: A new bulge test technique for the determination of Young's modulus and Poisson's ratio of thin films. *J. Mater. Res.* **7,** 3242 (1992).
26. Y. Xiang, X. Chen, and J.J. Vlassak: The plane-strain bulge test for thin films. *J. Mater. Res.* **20,** 2360 (2005).
27. S.J. Martin, J.P. Godschalx, M.E. Mills, E.O. Shaffer, and P.H. Townsend: Development of a low-dielectric constant polymer for the fabrication of integrated circuit interconnect. *Adv. Mater.* **12,** 1769 (2000).

28. D.W. Zheng, Y.H. Xu, Y.P. Tsai, K.N. Tu, P. Patterson, B. Zhao, Q.Z. Liu, and M. Brongo: Mechanical property measurement of thin polymeric-low-dielectric constant films using bulge testing method. *Appl. Phys. Lett.* **76,** 2008 (2000).
29. Y. Xiang and J.J. Vlassak: Bauschinger effect in thin metal films. *Scripta Mater.* **53,** 177 (2005).
30. ASTM E92, Standard Test Method for Vickers Hardness of Metallic Materials (ASTM International, West Conshohocken, PA, 1987).
31. D. Tabor: *The Hardness of Metals* (Clarendon Press, Oxford, U.K., 1951).
32. Y. Lin, Y. Xiang, T.Y. Tsui, and J.J. Vlassak: Octamethylcyclotetrasiloxane (OMCTS) based PECVD low-k organosilicate class (OSG) thin films. Part II: Mechanical properties and fracture (2005, unpublished).
33. K.L. Johnson: *Contact Mechanics* (Cambridge University Press, Cambridge, MA, 1985).